International Journal of Solids and Structures 50 (2013) 1164–1176

Contents lists available at SciVerse ScienceDirect

International Journal of Solids and Structures

journal homepage: www.elsevier.com/locate/ijsolstr

Metallic sandwich panels subjected to multiple intense shocks

Hamid Ebrahimi, Ashkan Vaziri *

Department of Mechanical and Industrial Engineering, Northeastern University, Boston, MA, United States

ARTICLE INFO

Article history:
Received 14 May 2012
Received in revised form 7 December 2012
Available online 11 January 2013

Keywords:
Sandwich panels
Honeycomb core
Folded plate core
Multiple shocks
Ductility
Dynamic response

ABSTRACT

The mechanical response and fracture of metal sandwich panels subjected to multiple impulsive pressure loads (shocks) were investigated for panels with honeycomb and folded plate core constructions. The structural performance of panels with specific core configurations under multiple impulsive pressure loads is quantified by the maximum transverse deflection of the face sheets and the core crushing strain at mid-span of the panels. A limited set of simulations was carried out to find the optimum core density of a square honeycomb core sandwich panels under two shocks. The panels with a relative core density of 4%–5% are shown to have minimum face sheet deflection for the loading conditions considered here. This was consistent with the findings related to the sandwich panel response subjected to a single intense shock. Comparison of these results showed that optimized sandwich panels outperform solid plates under shock loading. An empirical method for prediction of the deflection and fracture of sandwich panels under two consecutive shocks – based on finding an effective peak over-pressure – was provided. Moreover, a limited number of simulations related to response and fracture of sandwich panels under multiple shocks with different material properties were performed to highlight the role of metal strength and ductility. In this set of simulations, square honeycomb sandwich panels made of four steels representing a relatively wide range of strength, strain hardening and ductility values were studied. For panels clamped at their edge, the observed failure mechanisms are core failure, top face failure and tearing at or close to the clamped edge. Failure diagrams for sandwich panels were constructed which reveal the fracture and failure mechanisms under various shock intensities for panels subjected to up to three consecutive shocks. The results complement previous studies on the behavior and fracture of these panels under high intensity dynamic loading and further highlights the potential of these panels for development of threat-resistant structural systems.

1. Introduction

Threat-resistant structures that can withstand extreme loading conditions (e.g. impact, blast, thermal shock) and sustain their functionality are critical in both military and industrial settings. Development of such systems requires innovative design and manufacturing approaches to create high performance multifunctional materials and structural systems (Ajdari et al., 2012; Chen and Pugno, 2012; Fan et al., 2008; Latourte et al., 2012; Xiong et al., 2012b; Qiao et al., 2008). Examples of such developments are cellular structures with functionally graded and hierarchical structural organization, which are shown to have superior mechanical behavior compared to engineered cellular structures at the same overall mass (Ajdari et al., 2012; Ajdari et al., 2011). Another example is the ongoing efforts in development of sandwich panels with low density core constructions (Evans et al., 2010; Kishimoto and Shinya, 2001; Wadley et al., 2010, 2003; Xiong et al., 2011a, 2010). These panels are considered as promising candidates for development of impact- and explosion resistant structures (Cui et al., 2012; Dharmasena et al., 2008; Mori et al., 2007; Qin and Wang, 2009; Qiu et al., 2004; Rathbun et al., 2006; Xue and Hutchinson, 2004b). In fact, well-designed sandwich panels generally undergo smaller deflection under shock loading and also sustain higher intensity of shock prior to failure compared to solid plates of the same mass (Dharmasena et al., 2011; Hutchinson and Xue, 2005; Rabczuk et al., 2004; Vaziri and Hutchinson, 2007). The desirable mechanical performance of metal sandwich panels, combined with their multifunctional advantages (Evans et al., 2001; Wadley, 2006), makes them a unique candidate for development of low weight multifunctional structural systems.

The current studies related to impact mechanics and blast resistant sandwich panels all consider a single impulsive pressure loading (shock) or single projectile loading impinged on the panel. However, the application of sandwich panels in critical structures requires consideration of other possible events and loading scenarios. Examples of such scenarios are: (i) impingement of multiple shocks, (ii) shock loading followed by projectile impact (for

* Corresponding author. Tel.: +1 (617) 373 3474; fax: +1 (617) 495 9837.
E-mail address: vaziri@coe.neu.edu (A. Vaziri).

0020-7683/$ - see front matter © 2013 Elsevier Ltd. All rights reserved.
http://dx.doi.org/10.1016/j.ijsolstr.2012.12.013

example due to debris that becomes airborne as the shock wave travels towards the structure),(iii) multiple impacts by non-explosive projectiles (Gomez and Shukla, 2001; Yang and Bifeng, 2006; Yang et al., 2009), (iv) shock or projectile loading followed by an internal fire (e.g. World Trade Center Collapse in 2011 (Bazant and Zhou, 2002; Eagar and Musso, 2001)) and (v) shock or projectile loading followed by internal explosion (e.g. in pipeline networks and fuel tanks). Here we focus on the first scenario mentioned above which can occur due to multiple explosions in a combat zone (i.e. improvised explosive devices, bombs), underwater mine explosions, where one explosion could lead to a consequential explosion of nearby mines, or due to subsequent explosions resulting from an initial explosion in factories and industrial settings. One specific example related to this latter scenario is progressive failure and escalation in gas and oil pipelines or petrochemical facilities, where an initial explosion results in subsequent explosions, resulting in transmission of a complex loading scenario to surrounding structures (Makhutov et al., 1992; Roodselaar and Ward, 2004; Thomas, 2008).

The current work specifically studies the performance and failure of all metal sandwich panels impinged by multiple shocks and compares the results with the performance of the counterpart solid plate of same mass. To model shock loading, two different methods have been previously explored. The first method is based on applying uniform pressure history, $P(t) = P_0 e^{-t/t_0}$ for $t > 0$, to the surface of the top face of the panel, where P_0 and t_0 denote the peak overpressure and decay time associated with shock. The second method assigns an initial momentum/area, I, to the face of the sandwich towards the shock. In the first method, the momentum/area transferred to the panel is approximately equal to the impulse/area associated with the applied pressure history, $I = \int_0^\infty P dt = P_0 t_0$, as the momentum associated with the reaction forces at the support are negligible over the period shocks act on the panels (Vaziri and Hutchinson, 2007). In the present work, shocks are modeled by applying time-dependent pressure pulses in all the simulations (first method), which gives more realistic predictions, especially for core crushing since the crushing occurs early in the deformation history (Vaziri et al., 2007). $t_0 = 10^{-4}$ s = 0.1 ms was selected, which is a typical time duration for shock waves generated due to blast and is short compared to the overall response time of the plates (generally 1–10 ms). We have also neglected the fluid–structure interaction (e.g. air or water medium was not included in the numerical models) and carried out finite element simulations to predict the structural response and performance of sandwich panels after the shock is transferred to the panel face sheet. The simulations, in effect, model the behavior of panels in stage II and stage III of the response as defined by Fleck and Deshpande (2004). It should be noted that the provided results can be linked to air or water blast scenarios, at least approximately, according to the approach originally proposed for water blasts by Taylor (1963) and developed more fully for sandwich plates by Liang et al. (2007) and as extended by Kambouchev et al. (2006) to air blasts.

Fig. 1 shows two sandwich panel configurations considered in the present work, one panel has a square honeycomb core and the other has a folded plate core running perpendicular to the edges. Following several earlier studies (Vaziri and Hutchinson, 2007; Vaziri et al., 2006; Xue and Hutchinson, 2004a), panels are considered that are infinite in one direction and of width $2L$ in the other direction with fully clamped conditions along the two infinite edges. Sandwich panel geometry, material, and the boundary conditions of the panels are discussed in Section 2. In Section 3, we present detailed numerical simulations to study the response of square honeycomb and folded sandwich panels subject to multiple shocks. In Section 4, we present a parametric study on the response of square honeycomb panels with different core relative densities.

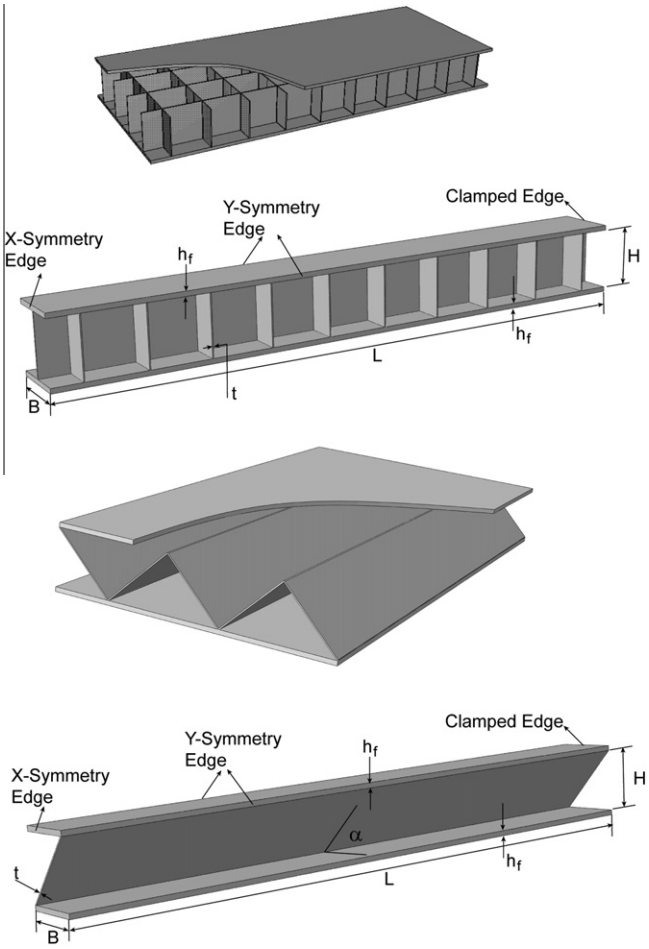

Fig. 1. Schematic diagrams of metal sandwich panel configurations and the corresponding computational models of the sandwich panel cells. The width of the panels is $2L$ and only half of the panels unit cell were modeled, while symmetry conditions were applied in both in-plane directions.

In this set of calculations, the total mass of the panel was constant, so the trade-off of increasing the core relative density was to thin the face sheets.

In Section 5, we studied the failure of honeycomb sandwich panels under multiple shock impingements. Finally, in Section 6, following the work of Vaziri et al. (2007), we performed a limited number of calculations to study the role of material behavior on the deformation and fracture response of panels against shock loading. The behavior of sandwich panels made from four steels – that represent a relatively wide range of strength, hardening and ductility values – were simulated and analyzed. The materials studied in this section are: AH36 with low ductility, HY80 high strength steel with low strain hardening, AL6XN stainless steel with intermediate yield strength, high strain hardening and high ductility, and DH36 intermediate strength steels with high ductility. The material properties for the four steels considered are briefly discussed in Section 2. The conclusions are drawn in Section 7.

2. Plate geometries and material specifications

Both core topologies are of height, H, web thickness, t, and have top and bottom face sheets of equal thickness, h. The square honeycomb core has web spacing B in both in-plane directions. The folded plate core has an inclination angle, α, such that the spacing of the folds in the y-direction is $B = t/\sin\alpha + H/\tan\alpha$. Core relative

density is defined as the volume fraction of the core that is occupied by the webs and is denoted by ρ_c, where

$$\rho_c = 2\frac{t}{B} - \left(\frac{t}{B}\right)^2 \quad \text{for the square honeycomb core} \tag{1}$$

$$\rho_c = \frac{t}{t + H\cos\alpha} \quad \text{for the folded plate core} \tag{2}$$

The mass/area of the sandwich panel is $M = \rho(2h + \rho_c H)$. By specifying L, M and ρ, the geometry of honeycomb sandwich panels is fully determined by ρ_c, H/L, B/H and L and the geometry of the folded plate core sandwich panels is fully determined by ρ_c, H/L, α and L. In our simulations, all panels have half-width, $L = 1$ m, and mass/area, $M = 156\ \text{kg m}^{-2}$, which is the same mass/area of solid plate with thickness equal to 20 mm. The core thickness of both types of sandwich plates is fixed at $H/L = 0.1$, and the web spacing of the square honeycomb is fixed at $B/H = 1$ while the folded plate cores have $\alpha = 45°$ such that $B/H \cong 1$. Because of symmetry, numerical simulations of the response are based on models of one unit cell of the sandwich panel with periodic boundary condition (as depicted in Fig. 1). Full three-dimensional models were constructed with detailed meshing of the core as reported in Xue and Hutchinson (2004a) and Vaziri et al. (2006). At least four 8-node brick elements were employed through the thickness of each face sheet, which captures early stages of necking with acceptable fidelity (Vaziri et al., 2006).

In Section 3, we studied the mechanical response of square honeycomb and folded plate core sandwich panels made of HY80 steel – which is a high strength steel with low strain hardening with Young's modulus, $E = 200$ GPa, Poisson's ratio $\nu = 0.3$ and density $\rho = 7800\ \text{kg m}^{-3}$ under multiple shocks. The true stress-plastic strain response displayed in Fig. 2A for HY80 is representative of the material response at a tensile strain rate of 100/s as adopted from Meyer et al. (2000). Material strain rate dependence is not included for metal sandwich panels made of HY80, since sufficient data does not exist in the literature. In Section 4, we studied the role of core density on the response of square honeycomb made of HY80 steel to obtain the optimized configuration of sandwich panels. In Section 5, we studied failure mechanisms of sandwich panels under multiple shocks. Panels with square honeycomb cores are known to have higher damage tolerance under high intensity dynamic loading than those with folded plate cores in that they can withstand loads much larger than those at which the first signs of fracture appear. Here, we study the failure of square honeycomb panels under multiple shock loading made from four steels (AH36, HY80, AL6XN, DH36) that represent a relatively wide range strength, hardening and ductility behavior. Young's modulus, Poisson's ratio and the density of all the steel materials are the same and have the value as stated above. Fig. 2A presents tensile true stress-logarithmic strain curves of the four materials. Fig. 2B presents the effective plastic strain at failure, $\left(\varepsilon^p_{eff}\right)_c$, plotted as a function of the triaxiality ratio, σ_m/σ_e, where $\sigma_m = \sigma_{kk}/3$ is the mean stress, $\sigma_e = 3s_{ij}s_{ij}/2$ is the effective stress and s_{ij} is the stress deviator for all materials other than HY80, since to our best knowledge data for HY80's ductility is not available in the open literature. In Section 5, a parametric study will be presented for sandwich panels made of HY80 using the fracture strain as a variable to investigate the role of material ductility on the fracture of sandwich panels made of this material.

For AH36, the true stress-plastic strain response and the fracture locus are taken from Lee and Wierzbicki (2005). The tensile data for AL6XN is provided by Nahshon et al. (2007) and is similar to data given by Nemat-Nasser et al. (2001). For DH36, the (Johnson and Cook, 1983) plasticity model is employed for representing the stress–strain response of the material, as provided by Nemat-Nasser and Guo (2003). Temperature variations are neglected and room temperature properties are used yielding the following relation between the effective stress and effective plastic strain:

$$\sigma_e = 470\left(1 + 1.5\left(\varepsilon^p_{eff}\right)^{0.4}\right)\left(1 + 0.015\ln\left(\dot{\varepsilon}^p_{eff}/1s^{-1}\right)\right)(\text{in MPa}), \quad \text{at}$$

the effective strain rate of $\dot{\varepsilon}^p_{eff}$. The plot shown in Fig. 2A for DH36 is at the effective strain rate $\dot{\varepsilon}^p_{eff} = 100\ \text{s}^{-1}$. Material strain rate dependence is accounted in calculations for DH36, if not mentioned otherwise. The failure locus data for both DH36 and AL6XN are based on fitting experimental data to the Johnson–Cook shear failure model (Vaziri et al., 2007). As will be discussed in the following sections, no failure was observed in the sandwich panels made of AL6XN and DH36, for the range of shock intensities considered in this study.

3. Numerical analysis of sandwich panels subjected to multiple intense shocks

In this section, detailed results on the deformation of honeycomb and folded plate core sandwich panels are presented for plates made of HY80 steel. The panel geometry was constructed directly in the graphical user interface of the software and the boundary conditions were applied. To model loading of multiple

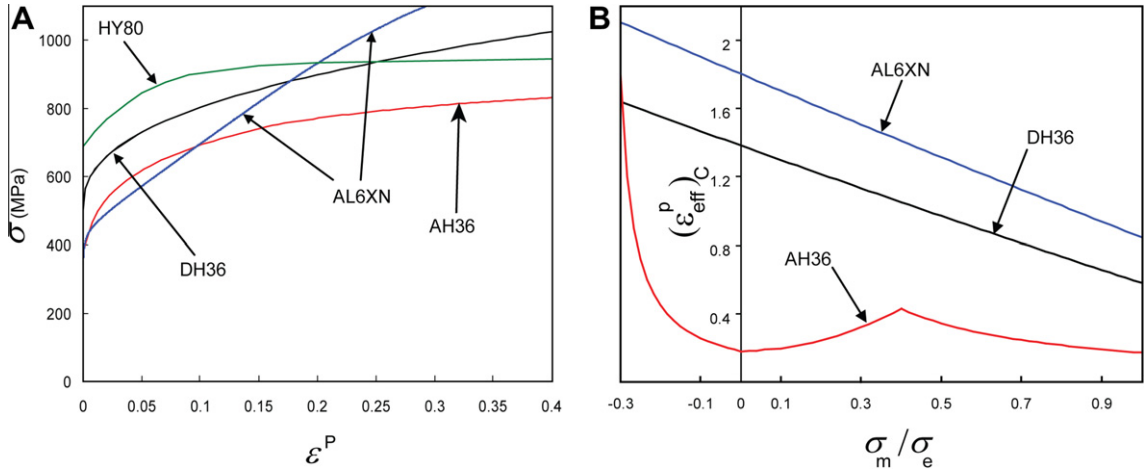

Fig. 2. (A) True stress-plastic strain response of the four steels considered in this study. (B) Failure locus for three of the four steels. The failure data for HY80 is not available in the literature.

shocks, we need to also define the separation time between the loading from different shocks (e.g. time between two peak pressures). Fig. 3A shows the schematic diagram of half of a sandwich panel subjected to two consecutive shocks with peak over-pressures for the first and second shocks denoted by P_1 and P_2, respectively. The separation time between the two peak over-pressure is denoted by t_s. In the numerical model, the pressure loading for different values of P_1, P_2 and t_s was then added manually to the input file prior to the analysis. The material failure and panel fracture were not considered here and will be studied in Section 5. All results have been determined with fully clamped boundary conditions and the panel geometry as discussed in Section 2. The simulations were carried out using ABAQUS/Explicit 6.10.

3.1. Role of separation time between consecutive shock events

As the first step, we carried out a systematic study on the role of t_s (the separation time between two consecutive shocks) on the response and deformation of solid and sandwich panels. In the calculations presented in this section, $P_1 = 50$ MPa, $t_0 = 10^{-4}$ s, while t_s and P_2 were systematically varied. In each calculation, we measured the time history of the deflection of the bottom face sheet of the sandwich panels under two shock impingements. Fig. 3B shows the maximum normalized deflections of the bottom face sheet, δ_{bot}^{max}/L, of the honeycomb sandwich panel with $\bar{\rho}_c = 0.04$ made of HY80 versus the normalized time between the two shocks, $\bar{t}_s = t_s/(L/\sqrt{(\sigma_Y/\rho)})$ (Vaziri and Hutchinson, 2007; Xue and Hutchinson, 2004a). The results for the maximum deflection of the counterpart solid panel are also plotted for comparison. In this

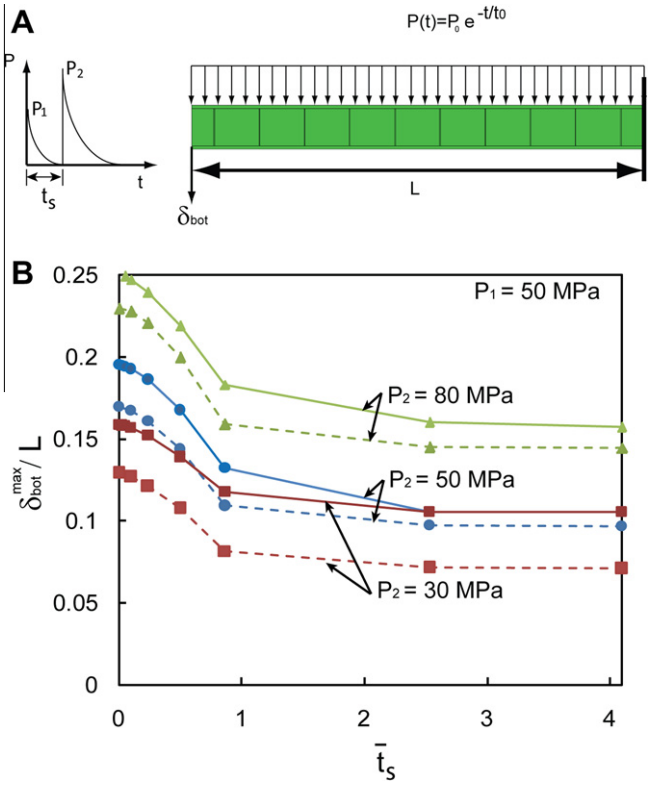

Fig. 3. (A) Schematic diagram of a square honeycomb sandwich panel subjected to two shocks with peak over pressures of P_1 and P_2. (B) Normalized maximum deflection of the bottom face of the square honeycomb sandwich panel with $\bar{\rho}_c = 0.04$ made of HY80 (dashed lines) and the counterpart solid plate of same mass/area (solid lines) versus normalized shock time subjected to two shocks. No failure criterion is incorporated and the square honeycomb core panel has $M = 156$ kg/m^2, $L = 1$ m and $\bar{\rho}_c = 0.04$.

relation σ_Y and ρ are yield strength and density of the panel material, respectively. For a panel made from HY80 with $L = 1m, L/\sqrt{\sigma_Y/\rho} \cong 3.4$ ms.

The results show that for loading with $\bar{t}_s > 1$, the response of both sandwich and solid panels is approximately independent of the value of $\bar{t}_s$. In this case, the response of the panel to two shocks is effectively uncoupled and the two shocks can be treated as two isolated loadings or events (i.e. the second shock impinges the panel after it has come nearly to rest after the first shock impingement). It should be noted that this finding appears to be independent of the panel configuration, and only depends on the material behavior, namely the yield strength and density of the panel material.

For $\bar{t}_s < 1$, the maximum deflection of the panel increases as the duration between two shocks becomes shorter. When $\bar{t}_s$ approaches zero, the maximum deflection of the panel under two shocks becomes equal to the maximum deflection of a panel subjected to one shock with over-pressure equal to $P_1 + P_2$, as expected. It should be noted that for all loading conditions, the honeycomb panel undergoes smaller deformation compared to its solid panel counterpart.

3.2. Time-response of sandwich panels impinged by two shocks

In the calculations presented in this section, we chose $t_s = 8$ ms which corresponds to $\bar{t}_s \cong 2.3$. While $t_s = 8$ ms is a short time lag between the two shocks, based on the results presented in Fig. 3B and discussed in Section 3.1, this insures that panels are at rest (except for low amplitude elastic vibrations) before the second shock impinges on the structure. It should be noted that having very short time difference between two shocks with $\bar{t}_s < 1$ is perhaps not a common scenario and thus is not considered further in this work.

Fig. 4 shows normalized deflection of the bottom face (denoted by δ_{bot}/L), of both honeycomb and folded sandwich panels with $\rho_c = 0.04$ and made from HY80 subjected to two shocks as a function of dimensionless time, $t/(L/\sqrt{(\sigma_Y/\rho)})$. Here, t was measured from the time that the first shock impinges the panel (i.e. $t = 0$ at the occurrence of the first over-peak pressure, P_1). Also shown is the time history of core crushing strain at the mid-span of the sandwich panels, defined as the ratio of core height in the deformed configuration to the original height, and denoted by ε_c. By eliminating the local bending of the top and bottom face sheet, core crushing strain can be estimated from $\epsilon_c \cong (\delta_{top} - \delta_{bot})/H$, where δ_{top} is the top face displacement.

For each core type, the figure presents results for three sets of loadings. For honeycomb panels, $P_1 = 100$ MPa and constant in all calculations, and P_2 was selected as 80,100, and 130 MPa in the three simulations. For folded panels, $P_1 = 80$ MPa and P_2 was selected as 60, 80, and 100 MPa. In our simulations, we generally used lower intensity of loading for folded panels compared to their honeycomb panel counterpart. The reason is that folded panels in general sustain lower loading intensity prior to failure compared to their honeycomb panel counterpart, as discussed in details in our previous publication (Vaziri et al., 2007). For example, for the folded panel considered here, the loading of $P_1 = 100$ MPa and $P_2 = 100$ MPa, leads to significant necking at the clamped edges of the panels, thus, making the simulation results inaccurate.

The deflection induced by the second shock is considerably smaller than the deflection due to the first shock with the same over-pressure intensity for both core types. For instance, the normalized maximum deflection of bottom face of honeycomb sandwich panel in the first shock subjected to load with $P_1 = 100$ MPa is $\frac{\delta_{bot}^{max}}{L} \cong 0.16$, whereas the second shock with $P_2 = 100$ MPa adds only 0.04 to the maximum deflection value. The folded core

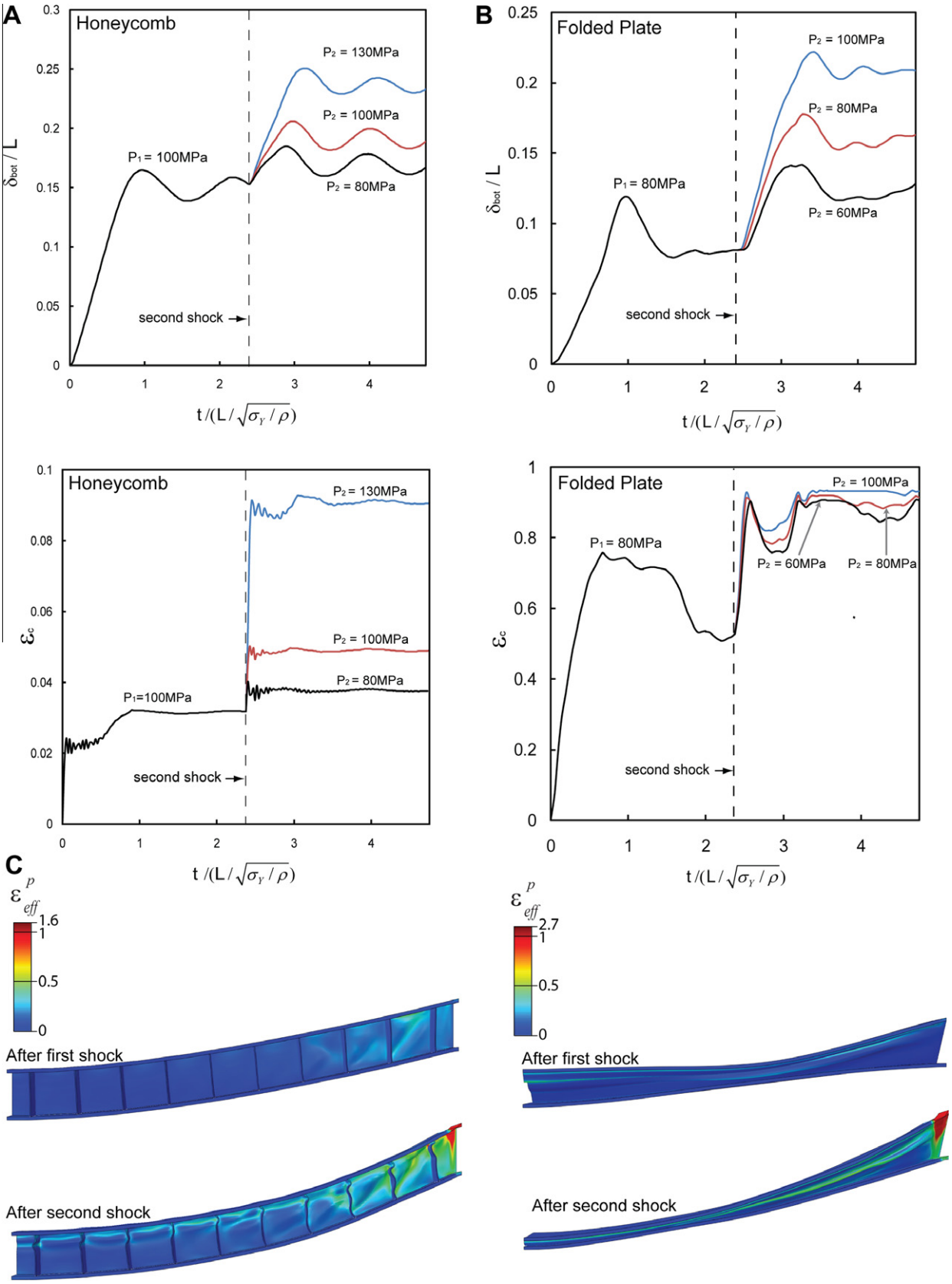

Fig. 4. Normalized bottom face deflection and core crushing strain at the center of the panel versus normalized time for (A) a square honeycomb sandwich panel and (B) a folded plate sandwich panel. In each plot, the peak over-pressure of the first shock is the same for all panels, but varies for the second. (C) Deformed configuration of the sandwich panels after the first and second shock. The deformed configurations are shown for a square honeycomb subjected to $P_1 = 100$ and $P_2 = 130$ MPa and for a folded plate sandwich panel subjected to $P_1 = 80$ and $P_2 = 100$ MPa. The panels made of HY80 and have $\bar{\rho}_c = 0.04$, $M = 156$ kg/m^2 and $L = 1$ m.

sandwich panel subjected to $P_1 = P_2 = 80$ MPa, has δ_{bot}^{max}/L of 0.12 and 0.18 after the first and second shock impingement, respectively. One reason is that the maximum deflection plotted here is larger than the residual displacement of the sandwich panels, as can be seen in Fig. 4A for a honeycomb sandwich panel and in Fig. 4B for a folded plate sandwich panel. The deformed configuration of sandwich panels after the first and second shock, as well as the distribution of the effective plastic strain in face sheets and cores are shown in Fig. 4C. For both sandwich panels, local necking of the top face sheet is observed after the second shock – for further discussion on dynamic necking, see Xue et al. (2008). Note that for the folded sandwich panel, the final core crushing strain for all three sets of loading is close to 1 as the core undergoes near-total crushing after the impingement of the second shock.

We carried out an additional set of simulations to study the role of shock impingement order on the sandwich panel response. The calculations were performed for the same sandwich panel configuration as Fig. 4. For the honeycomb, the calculations were carried out for the following loading conditions: (i) $P_1 = 80$ MPa and $P_2 = 130$ MPa and, (ii) $P_1 = 130$ MPa and $P_2 = 80$ MPa. This meant that shocks with the same peak over-pressures but in different orders were impinged on the structure. Note that the magnitude of the total momentum imparted to panels in two loading cases is similar. The first shock applies a momentum normal to the undeformed configuration of panel. The second shock is applied normal to the deformed configuration of the panel and generates momentum in both normal and tangential direction compared to the original undeformed configuration of the panel. The component of the momentum in the normal direction results in larger deformations. However, the contribution of the tangential component of the momentum is not negligible.

The response curves of the sandwich panels, as obtained from the detailed numerical simulations, are plotted in Fig. 5A. Loading (i) – where the second shock is more intense compared to the first shock – induces somewhat larger values of deflection and core crushing strain compared to loading (ii). Similar results are obtained for the deflection of folded panels, Fig. 5B. In both simulations, the folded plate core crushes almost completely. In the following section, we define an empirical *effective peak pressure*, P_{eff} for two consecutive shocks, which can be used to interpret the results presented in this section. As will be discussed later, loading (i) has a larger P_{eff} so it undergoes more deflection than loading (ii). Also the total crushing strain of honeycomb core in loading (i) is slightly higher than in loading (ii).

3.3. Panel deflection and crushing strain versus peak pressures

We carried out a parametric study on the effect of shock intensities on the maximum deflection and core crushing strain of sandwich panels. The simulations were carried out for honeycomb panels made of HY80 with core density $\bar{\rho}_c = 0.04$ impinged by two consecutive shocks with $t_s = 8$ ms ($\bar{t}_s \cong 2.3$). The over-peak pressures of two shocks denoted by P_1 and P_2 were varied between 0 and 130 MPa. As discussed by Xue and Hutchinson (2004a), the normalized maximum deflection of the sandwich panel impinged by a shock with peak over-pressure P_1 can be estimated from,

$$\frac{\delta_{bot}^{max}}{L} = A\frac{P_1 t_0}{M\sqrt{\sigma Y/\rho}} \tag{3}$$

assuming the material is sufficiently ductile to survive an intense blast. The dimensionless prefactor of the above equation, A, can be estimated from the numerical simulations of panel deformation under various shock intensities. For a honeycomb sandwich panel with core relative density 4%, $L = 1$ m, $M = 156\ \mathrm{kg}^{-2}$, $\sigma_Y = 690$ MPA, $\rho = 7800\ \mathrm{kgm}^{-3}$ and $A \approx 0.705$. For the counterpart solid plate of equal mass, $A \approx 0.895\ \mathrm{kg}^{-1}\ \mathrm{m}^2$, which shows that the solid plate undergoes higher deformation compared to the honeycomb sandwich panel. It should be emphasized that the value of P_1 used in calculating the above prefactors correspond to the shock intensity transmitted to the panels. Fluid–structure interaction results in lower intensity of imparted shock to sandwich panels compared to its solid plate counterpart for the same far field shock wave, especially when the shock is transmitted through water, as discussed in details in the current literature (Espinosa et al., 2006; Fleck and Deshpande, 2004; Jones, 1989; Latourte et al., 2012; Liang et al., 2007).

For panels subjected to two consecutive shocks with $\bar{t}_s > 1$, our numerical simulations show that the second shock loading with peak over-pressure, $P_2 < \frac{P_1}{2}$ does not result in considerable elevation of sandwich panel maximum deflection. Based on our parametric numerical simulations for $P_2 < \frac{P_1}{2}$, only a part of the momentum of second shock equal to $(P_2 - \frac{P_1}{2})t_0$ results in significant additional deformation of the sandwich panels. In this case, the maximum deflection of the sandwich panel can be estimated by adding the deflection associated with the first shock, P_1 and a part of the second shock momentum $(P_2 - \frac{P_1}{2})t_0$. Here, we define an empirical *effective peak pressure* denoted by $P_{eff} = P_1 + \{P_2 - \frac{P_1}{2}\}$ so that

$$\left\{P_2 - \frac{P_1}{2}\right\} = \begin{cases} 0 & \text{if} \quad P_2 < \frac{P_1}{2} \\ P_2 < \frac{P_1}{2} & \text{if} \quad P_2 < \frac{P_1}{2} \end{cases}$$

Thus,

$$P_{eff} = P_1 + \left\{P_2 - \frac{P_1}{2}\right\} = \begin{cases} P_1 & \text{if} \quad P_2 < \frac{P_1}{2} \\ P_2 + \frac{P_1}{2} & \text{if} \quad P_2 > \frac{P_1}{2} \end{cases} \tag{4}$$

By this definition, deflection of the honeycomb sandwich panel or solid plate under two consecutive shock loading can be estimated from,

$$\frac{\delta_{bot}^{max}}{L} = A\frac{P_{eff} t_0}{M\sqrt{\sigma Y/\rho}} \tag{5}$$

Fig. 6A and B shows the maximum deflection of bottom face of solid and honeycomb panels made of HY80 versus effective peak pressure, respectively. In each plot, the numerical results are presented for fifteen loading conditions with $P_2 < \frac{P_1}{2}$ and for over forty loading conditions with $P_2 < \frac{P_1}{2}$. The numerical results for loading conditions with $P_2 < \frac{P_1}{2}$ are shown by red markers. Each red marker corresponds to the results from several simulations, since in this case the intensity of second shock has no significant effect on the final deformation of the panels, as predicted by Eq. (5) above. In each plot, the empirical predictions from Eq. (5) is also plotted as a solid line. Overall, the results show acceptable agreement for both panels, while the difference between the numerical results and empirical predictions is more pronounced in the case of solid panels. This empirical relationship can be used to predict the behavior of sandwich panels subjected to two shocks, if the results for the response under single shock loading are available.

A limited set of numerical simulations were performed to explore whether the above approach could be extended to estimate the response of panels subjected to three and four consecutive shocks. We could not determine a simple empirical relationship that could present the response of panels under such loading conditions.

We carried out an additional set of simulations to decipher the role of material hardening on the behavior of sandwich panels under shock loading. In this set of calculations, we assumed the material to be elastic perfectly plastic with the same elastic properties and yield strength as HY80. This set of calculations eliminates the role of material hardening on the response of the panels. The results show that the material hardening has negligible effect on the response of the panels prior to any significant fracture. However, the maximum shock intensity that the panel can withstand noticeably depends on the hardening behavior of the metal. For

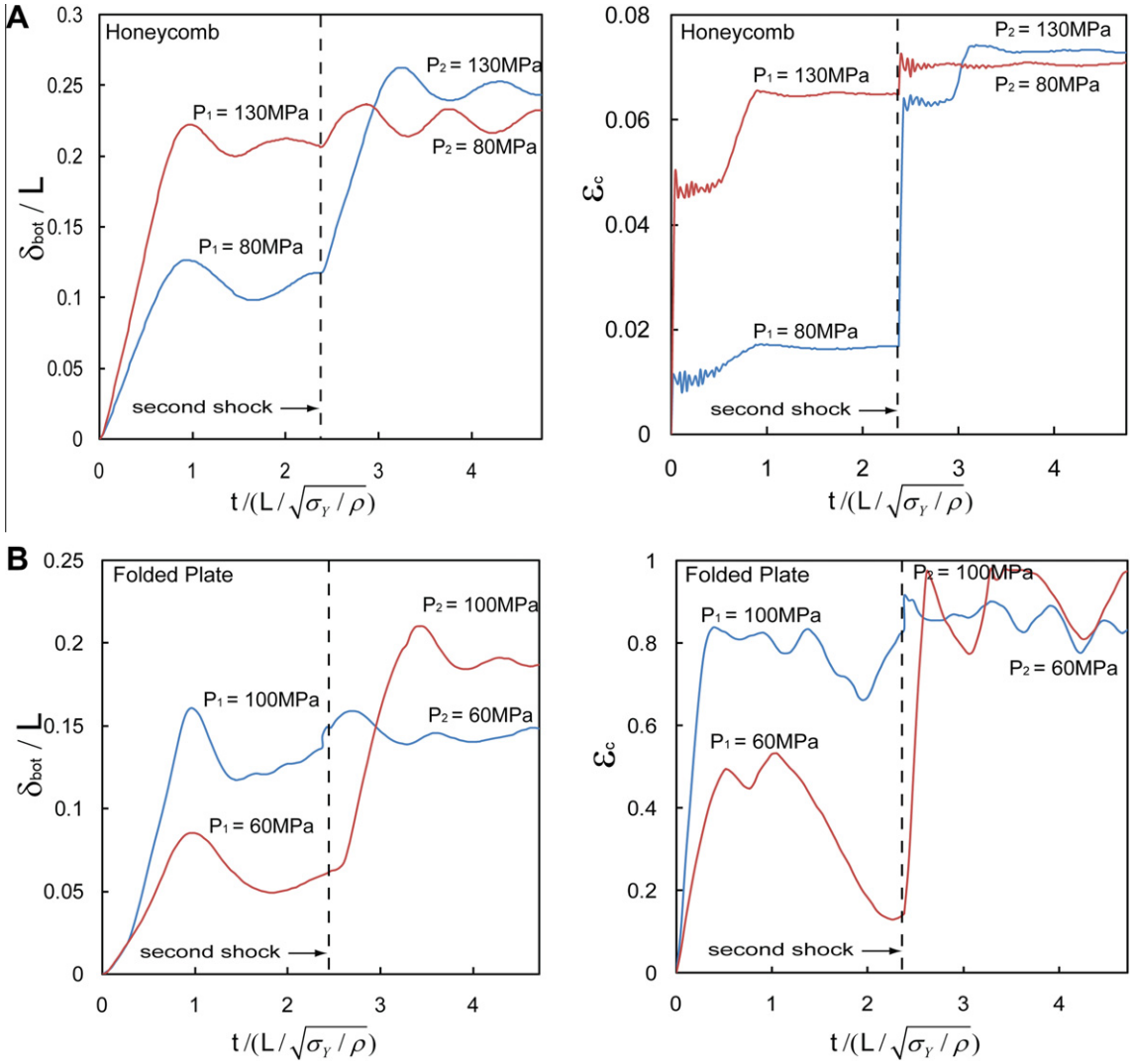

Fig. 5. Normalized bottom face deflection and core crushing strain at the center of the panel versus normalized time for (A) the square honeycomb sandwich panel and (B) folded plate sandwich panel. The panels made of HY80 and have $\bar{\rho}_c = 0.04$, $M = 156$ kg/m^2 and $L = 1$ m.

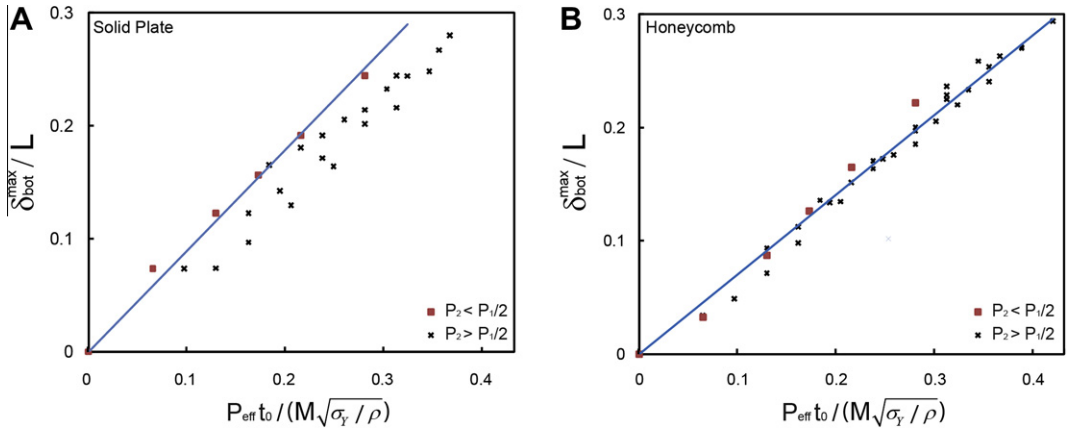

Fig. 6. Comparison between the numerical simulation results and the prediction from Eq. (5) for normalized maximum deflection (A) a solid plate and (B) the bottom face of square honeycomb sandwich panel subjected to two shocks. Both sandwich panel and solid plate are made of HY80 and have $M = 156$ kg/m^2 and $L = 1$ m. The square honeycomb sandwich panel has core relative density $\bar{\rho}_c = 0.04$. Solid lines show the theory results and markers indicate simulation outcomes. Results are presented for two loading cases, $P_2 < \frac{P_1}{2}$ and $P_2 < \frac{P_1}{2}$. For loading case, $P_2 < \frac{P_1}{2}$, each marker represents several simulation data points. The total number of data points in each figure is about sixty.

panels with no hardening, necking of the face sheets at low shock intensities was observed, which results in premature failure of the panels.

4. Optimized sandwich configuration

In this section, we carried out a parametric study of the effect of panel geometrical configuration on its response under two consecutive shocks. More specifically, we systematically varied the relative distribution of the face sheet's mass and core relative density and explored the role of core relative density on the overall response of the sandwich panels. The total mass of the panels was kept constant. This means that, for example, the trade-off in increasing the thickness of the face sheets is thinning of the core webs and thus, lowering the core relative density. The response of the panels under one high intensity shock and two consecutive shocks was obtained using detailed numerical simulations and compared to the response of the counterpart solid plate of equal mass. Previous optimization studies on the performance of metal sandwich panels with a similar configuration as the current study showed that honeycomb and folded plate sandwich panels with a core relative density of 4%–5% generally undergo minimum face sheet deflections under high intensity dynamic loading (Hutchinson and Xue, 2005; Xue and Hutchinson, 2004a). In this case, 20%–25% of the overall mass of the panel is distributed in the core. Core crushing, face sheet stretching and deformation, and local bending of the face sheets are the main deformation mechanisms of the sandwich panels which contribute to their overall deformation and response. For sandwich panels with very low core relative density (1%–2%), core crushing is significant. For sandwich panels with high core relative density (>6%), the face sheets undergo significant bending and stretching, while the core crushing is minimal. For panels with core relative density of 4%–5%, the contribution of all the mechanisms is relatively moderate, resulting in lower overall deformation of the panels (Vaziri et al., 2006). This panels are also shown to have maximum failure tolerance under high intensity dynamic loading (Vaziri et al., 2007).

In this section, we extend these investigations to sandwich panels subjected to two consecutive intense shocks. In our simulations, we consider square honeycomb sandwich panels with relative core density of 1%–8% made from HY80 steel. Similar to the previous section, material failure and fluid–structure interaction were not considered in the simulations and the calculations were carried out by keeping the total mass/area of the panels constant, $M = 156\ \mathrm{kg\ m^{-2}}$. Fig. 7A displays the normalized maximum deflection of the top face of the square honeycomb sandwich panels as a function of core relative density, $\bar{\rho}_c$. The first shock over-pressure was set at $P_1 = 100$ MPa, and the simulations were carried out for $P_2 = 0, 80, 100$ and 130 MPa. The set denoted by $P_2 = 0$ refers to sandwich panels subjected to a single shock with $P_1 = 100$ MPa. The maximum deflections of counterpart solid panels are also shown by a straight solid lines under each loading other than the highest shock intensity, $P_2 = 130$ MPa. A solid plate subjected to $P_2 = 130$ MPa undergoes significant necking close to their boundary, which makes the numerical results inaccurate.

Honeycomb sandwich panels with core relative density of 4%–5% have the minimum top face deflection under all loading conditions. When the panels are subjected to two shocks, the influence of core relative density becomes somewhat more significant. For instance, the maximum top face deflection of a panel with core relative density 4% is approximately 15% less than the maximum deflection of a panel with core relative density 1%, under single shock with $P_1 = 100$ MPa. This difference is 25%, when the panels are subjected to two consecutive shocks, $P_1 = 100$ MPa and $P_2 = 130$ MPa. It is noteworthy that the panels with moderate core relative density of 4%–5% noticeably outperform their counterpart solid panels. However, sandwich panels with very low or very high core relative densities undergo slightly larger deformations compared to their solid panel counterpart. Fig. 7B shows the core crushing strain at the mid span of the honeycomb sandwich panels as a function of core relative density for the same loading condition discussed above. As expected, for panels with a low core relative density, the core crushes significantly. Panels with core relative density above 4% have almost identical core crushing strain for all loadings.

Final deformed configurations of the square honeycomb sandwich panels with three core relative densities under two consecutive shocks, $P_1 = 100$ and $P_2 = 80$ MPa, are shown in Fig. 7C. For the panel with core relative density 1%, the core webs undergo significant crushing. For panels with the thinnest face sheets ($\bar{\rho}_c = 8\%$), top face undergoes extensive plastic bending into the core while the core webs undergo very little deformation. For the optimized configuration with $\bar{\rho}_c = 4\%$ the panel undergoes modest amount of face sheet bending and core crushing, leading to superior performance of the panels under shock loading. This is discussed in more detail in Vaziri et al. (2006).

5. Fracture and overall failure of honeycomb sandwich panels under multiple shocks

Vaziri et al. (2007) studied the failure mechanisms of all-metal folded and honeycomb sandwich panels subjected to an intense shock and provided fracture-shock intensity maps for clamped sandwich panels. The analogous study for composite sandwich panels was presented by Andrews and Moussa (2009), Latourte et al. (2011). Here, we expand these results to the case of all-metal honeycomb sandwich panels subjected to multiple consecutive shocks. As the first step, we studied the fracture behavior of honeycombs panels with $\bar{\rho}_c = 0.04$ made of HY80 subjected to up to three intense shocks. As discussed before the failure criterion for this steel alloy is not available and was modeled in this study by assuming that the local failure occurs if the effective plastic strain reaches a critical value, $(\varepsilon^P_{eff})_c$. This is the simplest form of fracture criterion for the purpose of numerical analysis. In the calculations, failed elements were removed using the approach available in ABAQUS/Explicit 6.10 (SIMULIA, Providence, RI). Additional sets of simulations were carried out for sandwich panels made of AH36, Al6XN and DH36, which represent a range of ductility and material properties, as described in Section 2. The failure criteria as presented in Section 2 for these steel alloys was used in these set of calculations.

It should be emphasized that as HY80 is a high-strength steel, its fracture strain is likely to be dependent on stress triaxiality (as for AH36, where fracture strain and mode strongly depends on the triaxiality – see Fig. 2), which is not considered here. Another limitation of this study is ignoring the failure of joints and connections (e.g. welding for metal panels), which was not modeled in the simulations. Joint strength is known to be a limiting factor for performance and strength of sandwich panels (Wadley et al., in press; Mori et al., 2009; Xiong et al., 2012a; Xiong et al., 2011b) and thus, further studies are required to address the role of connection and joint failure on the overall performance of panels under shock loading.

Fig. 8A shows the deformed configuration of the sandwich panel impinged by three consecutive shocks of equal peak over-pressure, 80 MPa, after it comes to rest following each shock event. In this set of simulations, $(\varepsilon^P_{eff})_c = 0.4$, representing relatively moderate ductility. The contour map displays the effective plastic strain distribution in the panel. After the first shock, the panel undergoes relatively little core crushing and no apparent failure and cracking. The second shock results in cracking of the core webs close to the clamped boundary condition. Impingement of the third shock

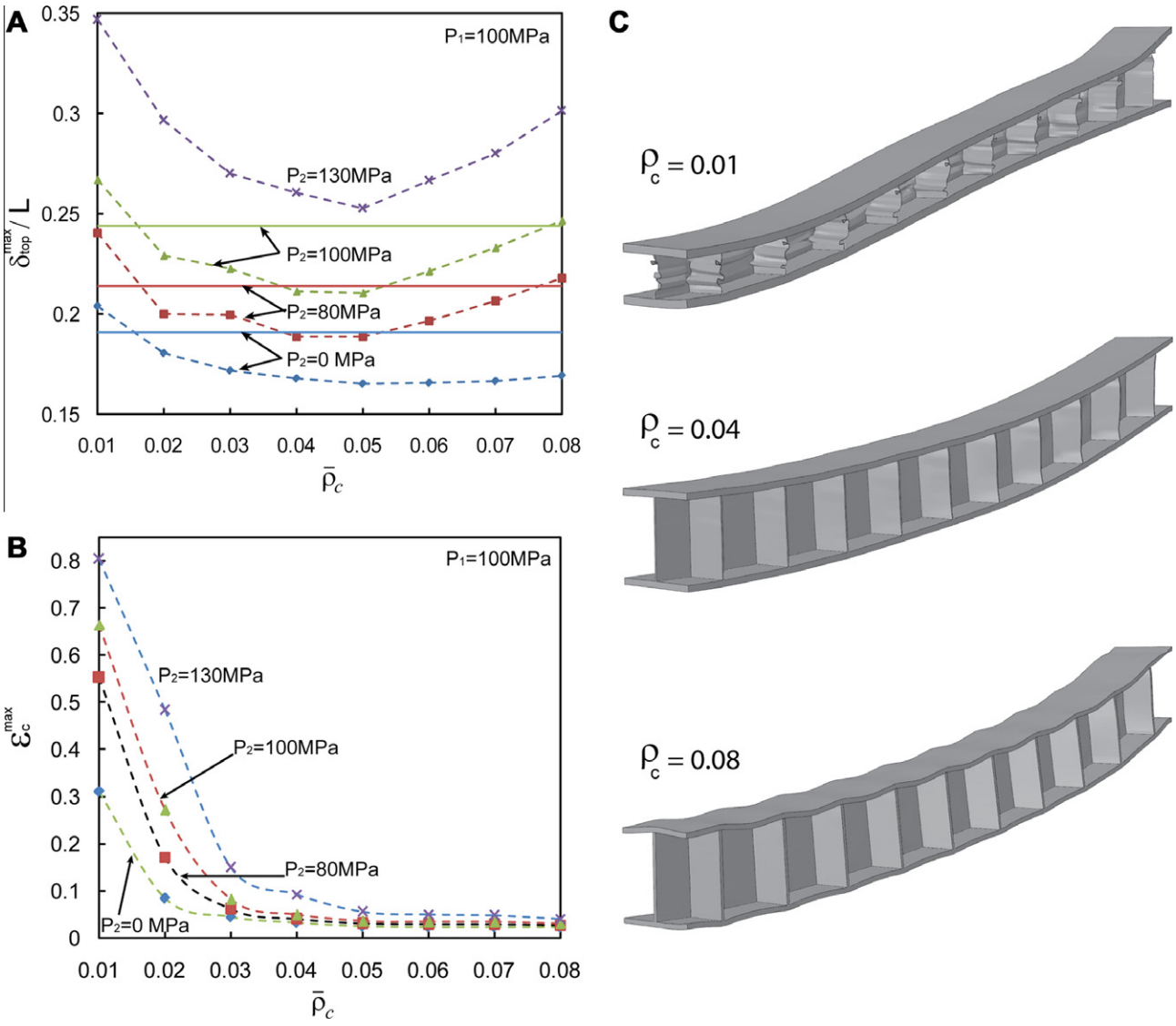

Fig. 7. (A) Normalized maximum deflection of the top face of the square honeycomb sandwich panel (dashed lines) and counterpart solid plate (solid lines) made of HY80 subjected to two shocks versus core relative density. (B) Maximum core crushing strain at the center of the square honeycomb sandwich plate versus the relative density of the core. (C) Deformed configuration of square honeycomb sandwich panels with three different core densities subjected to two consecutive shocks loading with peak over-pressures 100 and 80 MPA, respectively. In all diagrams, no failure criterion is incorporated for HY80, and sandwich panel has $M = 156$ kg/m^2 and $L = 1$ m.

causes excessive core failure close to the clamped boundary condition, as well as necking failure of top and bottom face fracture. The panel fully detaches from its support and becomes airborne (total failure).

To understand the role of material ductility and failure on the performance and fracture of sandwich panels, we studied the response and failure mechanisms of honeycomb sandwich panels made of HY80 with different hypothetical values of $(\varepsilon_{eff}^P)_c$. Fig. 8B shows the normalized maximum deflection of the bottom face of the sandwich panel versus effective peak pressure of shocks for $(\varepsilon_{eff}^P)_c = 0.2$, 0.4 and 0.6, representing a relatively large range of ductility. The results are presented for panels subjected to a single shock with peak over-pressure, P and panels subjected to two consecutive shocks with equal over-pressures, P. Considering many different possible loading conditions and shock intensities, we limited our study to panels subjected to two equi-peak shocks. Based on the empirical effective peak pressure defined in Section 3.2, for the first case $P_{eff} = P$ and for the second case $P_{eff} = \frac{3}{2}P$. As predicted by Eq. (5), the panel deformation increases approximately linearly by increasing the effective peak pressure prior to fracture. In Fig. 8B, for $P_{eff} < 90$ MPa the final deformation of the sandwich panel for all three sandwich panels are equal (i.e. for different values of $(\varepsilon_{eff}^P)_c$ considered here). In this range, no significant failure occurs in any of the panels. For more intense shocks, the core webs of the panel with $(\varepsilon_{eff}^P)_c = 0.2$ start to crack, leading to an increase in the overall deformation of the panel. This sandwich panel fails under a single shock with $P_{eff} = 110$ MPa or as it gets impinged with two shocks of $P_{eff} = 95$ MPa. Overall, the panel shows minimal ductility and tolerance to fracture, especially when it is subjected to two consecutive shocks. For a higher value of critical effective plastic strain, the sandwich panel fails at higher values of peak pressure and can sustain larger deflections prior total failure for both single shock and two shocks, as quantified in Fig. 8B.

In Fig. 9, we constructed a failure diagram for honeycomb sandwich panels with relative density $\rho_c = 0.04$ subjected to one shock or two or three equi-peak shocks. Again for the case of multiple shocks, we limited our study to the shocks with the same value of peak pressure. Sandwich panels made of AH36 and HY80 with three critical effective plastic strains, $\left(\varepsilon_{eff}^P\right)_c = 0.2,\ 0.4,$ and 0.6 were modeled. The diagram shows the overall mechanisms of

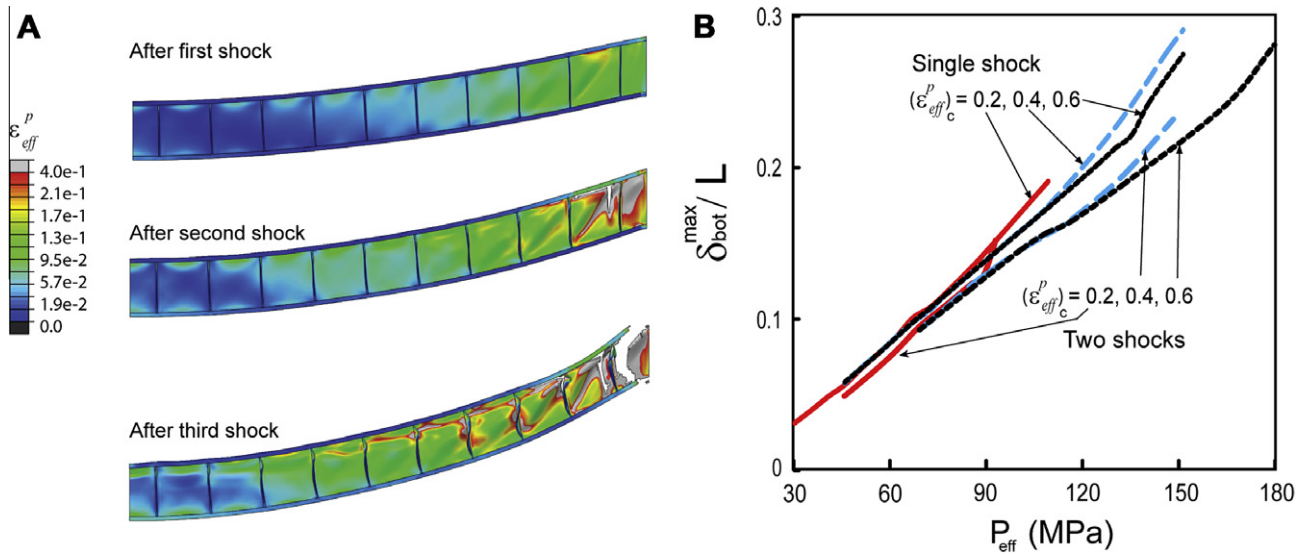

Fig. 8. (A) Final deformed configuration of square honeycomb panels after impingement of three consecutive shocks. Peak over-pressure of all shocks are equal to $P = 80$ MPa and critical plastic strain of HY80 was assumed to 0.4. (B) Normalized maximum deflection of the bottom face of the square honeycomb sandwich panel made of HY80 subjected to single or two equi-peak shocks versus the effective peak pressure. The results are plotted for three different critical plastic strains of HY80 steel, 0.2, 0.4 and 0.6. Note that for panels subjected to a single shock, the effective peak pressure is equal to the shock peak over-pressure. In all diagrams, sandwich panel has $M = 156$ kg/m^2, $L = 1$ m and $\rho_c = 0.04$.

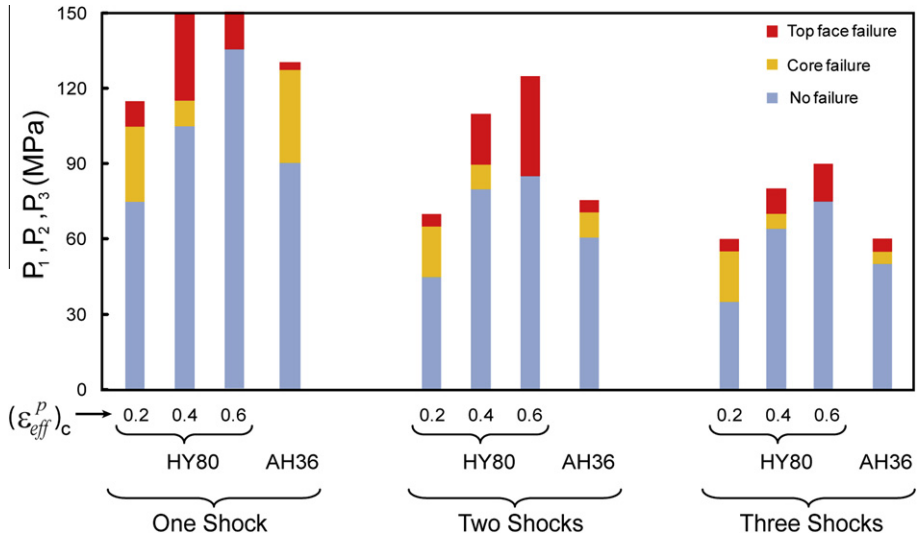

Fig. 9. Failure diagram of two square honeycomb sandwich panels made of HY80 or AH36 subjected to one/two/three equi-peak over-pressure shocks. Three critical effective plastic strain, 0.2, 0.4 and 0.6, are considered for failure of HY80. In all diagrams sandwich panels have $M = 156$ kg/m^2, $L = 1$ and $\rho_c = 0.04$.

fracture of the panel following each shock loading condition. The mechanisms identified are core failure and top face failure. Here, onset of core failure is identified when the total length of one continuous crack in the core becomes equal to the core height. The top face failure is defined as complete separation from the support. The bottom face failure results in detachment of the panel and its overall failure and is not considered as a separate failure mechanism in constructing this diagram. In all simulations, core failure precedes top face failure or occurs concurrently. For panels with low ductility (e.g. made of HY80 with $\left(\varepsilon^P_{eff}\right)_c = 0.2$), core failure is observed at much lower shock intensities compared to the top face failure. For panels with high ductility (e.g. made of HY80 with $\left(\varepsilon^P_{eff}\right)_c = 0.6$), the core and top face failure are concurrent. Moreover, for panels made of low ductility materials, the overall failure occurs at shock intensities that are slightly higher than the shock associated with the onset of top face failure. As the material becomes more ductile, the panel can tolerate a larger range of shock intensities in the presence of top face failure.

As an example, the first column of Fig. 9 presents the results for honeycomb sandwich panels made of HY80 with $\left(\varepsilon^P_{eff}\right)_c = 0.2$ and subjected to one shock loading. For shock with peak pressure, $P_1 < 75$ MPa, no apparent failure occurs in the sandwich panel (blue part of the bar, denoted by 'no failure'). For $P_1 > 75$ MPa, core failure was observed in the sandwich panels, denoted by the orange color in the column bar. For $P_1 > 110$ MPa, top face failure was observed (in addition to the core failure), shown by the red color in the column bar. Increasing P_1 to ~120 MPa, results in total failure of the panel, as the bottom face fails and the panel completely detaches from the supports. For sandwich panels with $\left(\varepsilon^P_{eff}\right)_c = 0.4$ and 0.6 subjected to one shock (i.e. the second and

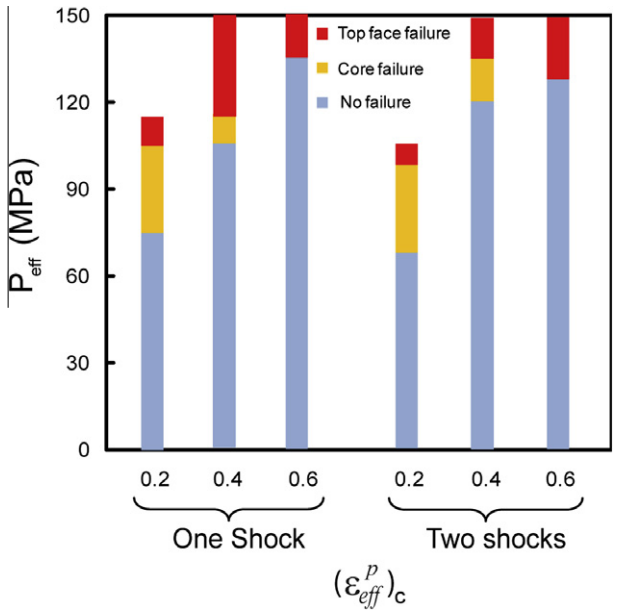

Fig. 10. Failure diagram of square honeycomb panel made of HY80 subjected to one or two consecutive equi-peak shocks presented in terms of effective peak pressure.

third columns), the onset of failure occurs at $P_1 = 105$ MPa and 135 MPa, respectively. For the sandwich panel with $\left(\varepsilon^{P}_{eff}\right)_c = 0.4$, the top face fails at $P_1 = 115$ MPa, which is slightly higher than the peak over-pressure corresponding to the onset of core failure. However, the bottom face fails at a considerably higher peak over-pressure that is out of the range of pressure shown in this diagram. For the sandwich panel with $\left(\varepsilon^{P}_{eff}\right)_c = 0.6$, core failure and top face failure occur almost simultaneously at $P_1 = 135$ MPa. Similar to sandwich panel with $\left(\varepsilon^{P}_{eff}\right)_c = 0.4$, the total failure occurs at peak pressure out of the range shown here. We have also presented the results for the counterpart sandwich panel made of AH36. As discussed in Section 2, AH36 has smaller yield strength and lower ductility compared to HY80 and approximately similar hardening behavior. In the simulations, AH36 fracture strain was dependent on the stress triaxility following the curve shown in Fig. 2. For the sandwich panel made of AH36, onset of core failure occurs at $P_1 = 90$ MPa, and total failure occurs at $P_1 = 130$ MPa. In general, panels made of AH36 can withstand more intensive shock loading than those made of HY80 with $\left(\varepsilon^{P}_{eff}\right)_c = 0.2$ before the first sign of failure. The calculations were repeated for sandwich panels subjected to two or three equi-peak shocks and the results are summarized in Fig. 9.

In Fig. 10, we have re-plotted the failure diagram for honeycomb panels made of HY80 subjected to one or two shocks in terms of effective peak pressure. When presented in terms of effective peak pressure, the results for panels subjected to one or two shocks are approximately identical. The results show that the effective peak pressure defined in Section 3.3 can be used to predict not only the deflection of square honeycomb sandwich panel subjected to two shocks but also its failure with reasonable accuracy.

6. Comparative performance of sandwich panels made from four different steels

In this section, the role of material properties on the overall response and failure of metal sandwich panels subjected to two shocks is investigated. Sandwich panels made from four steels characterized in Section 2: AH36, DH36, AL6XN and HY80 are considered. Of the four steels, DH36 is characterized most completely, and this is the only steel for which strain rate dependence data was available. To elucidate the role of DH36 strain rate dependence on the overall response of sandwich panels, we carried out two sets of simulations for sandwich panels made of DH36. In the first set, the DH36 behavior follows the relationship presented in Section 2 and is strain rate dependant. In the second set, DH36 behavior was assumed to be strain rate independent and presented by substituting $\left(\dot{\varepsilon}^{P}_{eff}\right)_c = 100\ s^{-1}$, as a constant in the same relationship. The panels made of HY80 were assumed to have $\left(\varepsilon^{P}_{eff}\right)_c = 0.4$. Concerns about the accuracy of the fracture criteria used for the individual steels have also been noted in Section 2. With these caveats in mind, the comparative study highlights important connections between material properties and panel performance under intense multi blast loading, as also discussed in depth in Vaziri and Xue (2007). Calculations were carried out for both square honeycomb and the folded plate sandwich panels, with relative core density, $\bar{\rho}_c = 0.04$. The panel dimensions and loading conditions are precisely as specified in Section 2.

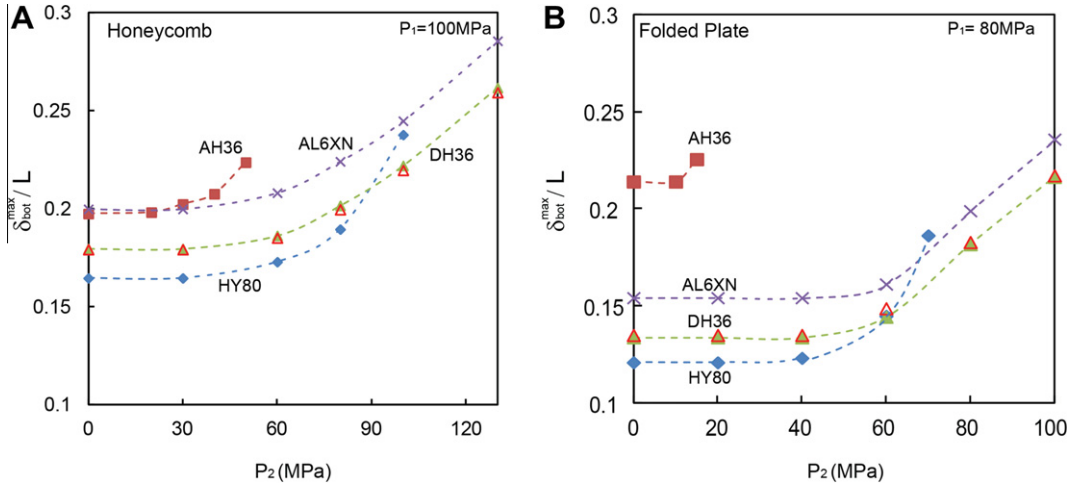

Fig. 11. Normalized maximum deflection of top face of the (A) square honeycomb and (B) folded plate core sandwich panels with $\rho_c = 0.04$ made of four steels subjected to two shocks versus peak over-pressure of the second shock. Two sets of results are presented for DH 36: with material strain rate dependence (green solid triangles) and with material strain rate independence (orange hollow triangles). For honeycomb sandwich panels, $P_1 = 100$ MPa and for folded plate panels, $P_1 = 80$ MPa. Critical effective plastic strain considered for failure of HY80 is equal to 0.4, and sandwich panels have $M = 156$ kg/m^2, $L = 1$ and $\rho_c = 0.04$.

Fig. 11 displays the dependence of the maximum bottom face deflection of the panels on the peak pressure of second shock for panels subjected to two shocks. The peak over pressure of the first shock impinged to the honeycomb and folded panels was P_1 = 100 MPa and 80 MPa, respectively. The curves were terminated at the peak pressure associated with total failure of the panel, as described earlier. The ductility of DH36 and AL6XN (see Fig. 2B) is sufficiently large that no failure occurs in either of the two types of panels over the range of shock peak pressure considered. By contrast, the limited ductility of AH36 and HY80 lead to panel failures at relatively low values of second shock peak pressure.

In general, panels made of higher strength steels, HY80 and DH36, undergo smaller deflections than the two lower strength steels. The first shock with peak pressure P_1 = 100 MPa results in appearance of core cracking and failure in the honeycomb panel made of AH36, but not in other panels. The honeycomb panels made of AH36 and AL6XN have similar deflection for $P_2 < 30$ MPa, where significant failure and cracking in AH36 panels occur, leading to an elevation in its overall deflection. For the folded plate panel, the top face almost fails after the impingement of the first shock with peak pressure P_1 = 80 MPa, resulting in minimum residual structural capacity of the panel. The deflection of the panel made of AH36 after the second shock impingement is significantly larger than the deflection of its counterpart panels made of AL6XN and its total failure occurs at P_2 = 18 MPa. It should be noted that AL6XN has strong strain hardening and its strength exceeds even that of HY80 at strains above 20% (Fig. 2B). However, in the simulations, the strains in the panels are generally limited to few percent and thus, the strain hardening of AL6XN has little influence in reducing the overall deflection. Considering the two sets of results presented for DH36, the strain rate dependence has minimal effect on the overall deflection of sandwich panels. This is conceivable, since the strain rate term in the relationship used to present DH36 material behavior is insignificant compared to other terms except under very large values of strain rate, which are not experienced by the sandwich panel material in the range of shock intensities considered in this study.

7. Conclusions

A limited set of calculations were carried out to study the response of sandwich panels with square honeycomb and folded plate core constructions made of four steels under multiple intense shocks (impulsive pressure loading). The dependence of panel deflection and failure modes on shock intensities were studied using detailed numerical simulations of the panel response. Comparisons with the counterpart solid panels were made to highlight the potential of sandwich panels as threat-resistant structural systems. An optimization study was conducted for square honeycomb core sandwich panels with different core relative densities but constant mass/area. In optimizing the structural designs against shock loading, it is generally desirable to achieve minimum deflection and fracture. The results indicate that a core relative density of 4%–5%, correspond to minimum deflection when panels are subjected to two shocks. This is in agreement with the results presented by Xue and Hutchinson (2004a) to minimize deflection of panels subjected to single shock loading.

An empirical relationship for estimating the response of panels under two consecutive, but isolated shocks were presented that allows predicting deformation and fracture of solid plates and square honeycomb panels with acceptable fidelity. However, additional studies are required to extend the applicability of such empirical relationship to panels made of different metallic alloys, as well as for loading cases comprised of more than two consecutive shocks.

Acknowledgments

The authors thank Professors John W. Hutchinson, Hamid Nayeb-Hashemi, Abdelmagid S. Hamouda, Jim Papadopoulos, and Andrew T. Myers for many constructive comments and helpful discussions. This work has been supported in part by the Qatar National Research Foundation (QNRF) under Award Number NPRP 09 - 145 - 2 - 061 and in part by the U.S. Department of Homeland Security under Award Number 2008-ST-061-ED0001. The views and conclusions contained in this document are those of the authors and should not be interpreted as necessarily representing the official policies, either expressed or implied, of the U.S. Department of Homeland Security.

References

Ajdari, A., Jahromi, B.H., Papadopoulos, J., Nayeb-Hashemi, H., Vaziri, A., 2012. Hierarchical honeycombs with tailorable properties. International Journal of Solids and Structures 49, 1413–1419.

Ajdari, A., Nayeb-Hashemi, H., Vaziri, A., 2011. Dynamic crushing and energy absorption of regular, irregular and functionally graded cellular structures. International Journal of Solids and Structures 48, 506–516.

Andrews, E.W., Moussa, N.A., 2009. Failure mode maps for composite sandwich panels subjected to air blast loading. International Journal of Impact Engineering 36, 418–425.

Bazant, Z.P., Zhou, Y., 2002. Why did the world trade center collapse? Simple analysis. Journal of Engineering Mechanics 128, 2–6.

Chen, Q., Pugno, N.M., 2012. In-plane elastic buckling of hierarchical honeycomb materials. European Journal of Mechanics – A/Solids 34, 120–129.

Cui, X., Zhao, L., Wang, Z., Zhao, H., Fang, D., 2012. Dynamic response of metallic lattice sandwich structures to impulsive loading. International Journal of Impact Engineering 43, 1–5.

Dharmasena, K.P., Wadley, H.N.G., Williams, K., Xue, Z., Hutchinson, J.W., 2011. Response of metallic pyramidal lattice core sandwich panels to high intensity impulsive loading in air. International Journal of Impact Engineering 38, 275–289.

Dharmasena, K.P., Wadley, H.N.G., Xue, Z., Hutchinson, J.W., 2008. Mechanical response of metallic honeycomb sandwich panel structures to high-intensity dynamic loading. International Journal of Impact Engineering 35, 1063–1074.

Eagar, T.W., Musso, C., 2001. Why did the world trade center collapse? Science, engineering, and speculation. Journal of the Minerals, Metals and Materials Society 53, 4.

Espinosa, H., Lee, S., Moldovan, N., 2006. A novel fluid structure interaction experiment to investigate deformation of structural elements subjected to impulsive loading. Experimental Mechanics 46, 805–824.

Evans, A.G., He, M.Y., Deshpande, V.S., Hutchinson, J.W., Jacobsen, A.J., Carter, W.B., 2010. Concepts for enhanced energy absorption using hollow micro-lattices. International Journal of Impact Engineering 37, 947–959.

Evans, A.G., Hutchinson, J.W., Fleck, N.A., Ashby, M.F., Wadley, H.N.G., 2001. The topological design of multifunctional cellular metals. Progress in Materials Science 46, 309–327.

Fan, H.L., Jin, F.N., Fang, D.N., 2008. Mechanical properties of hierarchical cellular materials. Part I: Analysis. Composites Science and Technology 68, 3380–3387.

Fleck, N.A., Deshpande, V.S., 2004. The resistance of clamped sandwich beams to shock loading. Journal of Applied Mechanics 71, 386–401.

Gomez, J.T., Shukla, A., 2001. Multiple impact penetration of semi-infinite concrete. International Journal of Impact Engineering 25, 965–979.

Hutchinson, J.W., Xue, Z., 2005. Metal sandwich plates optimized for pressure impulses. International Journal of Mechanical Sciences 47, 545–569.

Johnson, G.R., Cook, W.H., 1983. A constitutive model and data for metals subjected to large strains, high strain rates and high temperatures. In: Proceeding of Seventh International Symposium on Ballistics, The Netherlands, p. 7.

Jones, N., 1989. Structural Impact. Cambridge University Press, Cambridge.

Kambouchev, N., Noels, L., Radovitzky, R., 2006. Nonlinear compressibility effects in fluid–structure interaction and their implications on the air-blast loading of structures. Journal of Applied Physics 100, 063519.

Kishimoto, S., Shinya, N., 2001. New fabrication method for metallic closed cellular materials containing polymers. Materials and Amplify Design 22, 535–539.

Latourte, F., Grégoire, D., Zenkert, D., Wei, X., Espinosa, H.D., 2011. Failure mechanisms in composite panels subjected to underwater impulsive loads. Journal of the Mechanics and Physics of Solids 59, 1623–1646.

Latourte, F., Wei, X., Feinberg, Z.D., Vaucorbeil, A.D., Tran, P., Olson, G.B., Espinosa, H.D., 2012. Design and identification of high performance steel alloys for structures subjected to underwater impulsive loading. International Journal of Solids and Structures 49, 1573–1587.

Lee, Y.-W., Wierzbicki, T., 2005. Fracture prediction of thin plates under localized impulsive loading. Part II: Discing and petaling. International Journal of Impact Engineering 31, 1277–1308.

Liang, Y., Spuskanyuk, A.V., Hutchinson, J.W., 2007. The response of metallic sandwich panels to water blast, American Society of Mechanical Engineers, New York, ETATS-UNIS.

Makhutov, N.A., Serikov, S.V., Kotousov, A.G., 1992. Escalation failure of pipelines. Strength of Materials 24, 711–715.
Meyer, L.W., Krüger, L., Hahn, F.F., 2000. Influence of pre-deformation and strain rate on the flow behavior of HY80 steel. Emerging Technologies in Fluids, Structures and Fluid/Structure Interactions 1 (414), 295–300.
Mori, L., Queheillalt, D., Wadley, H., Espinosa, H., 2009. Deformation and failure modes of I-core sandwich structures subjected to underwater impulsive loads. Experimental Mechanics 49, 257–275.
Mori, L.F., Lee, S., Xue, Z.Y., Vaziri, A., Queheillalt, D.T., Wadley, K.P.D.H.N.G., Hutchinson, J.W., Espinosa, H.D., 2007. Deformation and fracture modes of sandwich structures subjected to underwater impulsive loads. Journal of Mechanics of Materials and Structures 2, 26.
Nahshon, K., Pontin, M.G., Evans, A.G., Hutchinson, J.W., Zok, F.W., 2007. Dynamic shear rupture of steel plates. Journal of Mechanics of Materials and Structures 2, 2049–2066.
Nemat-Nasser, S., Guo, W.-G., 2003. Thermomechanical response of DH-36 structural steel over a wide range of strain rates and temperatures. Mechanics of Materials 35, 1023–1047.
Nemat-Nasser, S., Guo, W.-G., Kihl, D.P., 2001. Thermomechanical response of AL-6XN stainless steel over a wide range of strain rates and temperatures. Journal of the Mechanics and Physics of Solids 49, 1823–1846.
Qiao, P., Yang, M., Bobaru, F., 2008. Impact mechanics and high-energy absorbing materials: review. Journal of Aerospace Engineering 21, 14.
Qin, Q.H., Wang, T.J., 2009. A theoretical analysis of the dynamic response of metallic sandwich beam under impulsive loading. European Journal of Mechanics – A/Solids 28, 1014–1025.
Qiu, X., Deshpande, V.S., Fleck, N.A., 2004. Dynamic response of a clamped circular sandwich plate subject to shock loading. Journal of Applied Mechanics 71, 637–645.
Rabczuk, T., Kim, J.Y., Samaniego, E., Belytschko, T., 2004. Homogenization of sandwich structures. International Journal for Numerical Methods in Engineering 61, 1009–1027.
Rathbun, H.J., Radford, D.D., Xue, Z., He, M.Y., Yang, J., Deshpande, V., Fleck, N.A., Hutchinson, J.W., Zok, F.W., Evans, A.G., 2006. Performance of metallic honeycomb-core sandwich beams under shock loading. International Journal of Solids and Structures 43, 1746–1763.
Roodselaar, A.V., Ward, J.W. 2004. Pipeline Risk Assessment Efforts in Upstream Operations – Results and Lessons Learned, CORROSION 2004, NACE International, New Orleans, LA.
Taylor, G.I., 1963. The pressure and impulse of submarine explosion waves on plates. In: Batchelor, G.K. (Ed.), The Scientific Papers of Sir Geoffrey Ingram Taylor, Volume III: Aerodynamics and the Mechanics of Projectiles and Explosions. Cambridge University Press, pp. 287–303.
Thomas, G.O., 2008. Some observations on explosion development in process pipelines and implications for the selection and testing of explosion protection devices. Process Safety and Environmental Protection 86, 153–162.
Vaziri, A., Hutchinson, J.W., 2007. Metal sandwich plates subject to intense air shocks. International Journal of Solids and Structures 44, 2021–2035.
Vaziri, A., Xue, Z., 2007. Mechanical behavior and constitutive modeling of metal cores. Journal of Mechanics of Materials and Structures 2, 1743–1761.
Vaziri, A., Xue, Z., Hutchinson, J.W., 2006. Metal sandwich plates with polymeric foam-filled cores. Journal of Mechanics of Materials and Structures 1, 95–128.
Vaziri, A., Xue, Z., Hutchinson, J.W., 2007. Performance and failure of metal sandwich plates subject to shock loading. Journal of Mechanics and Materials 2, 1947–1964.
Wadley, H.N.G., Børvik, T., Olovsson, L., Wetzel, J.J., Dharmasena, K.P., Hopperstad, O.S., Deshpande, V.S., Hutchinson, J.W., 2013. Deformation and fracture of impulsively loaded sandwich panels. Journal of the Mechanics and Physics of Solids 61, 674–699.
Wadley, H.N.G., 2006. Multifunctional periodic cellular metals. Philosophical Transactions of the Royal Society A: Mathematical, Physical and Engineering Sciences 364, 31–68.
Wadley, H.N.G., Dharmasena, K.P., He, M.Y., McMeeking, R.M., Evans, A.G., Bui-Thanh, T., Radovitzky, R., 2010. An active concept for limiting injuries caused by air blasts. International Journal of Impact Engineering 37, 317–323.
Wadley, H.N.G., Fleck, N.A., Evans, A.G., 2003. Fabrication and structural performance of periodic cellular metal sandwich structures. Composites Science and Technology 63, 2331–2343.
Xiong, J., Ma, L., Pan, S., Wu, L., Papadopoulos, J., Vaziri, A., 2012a. Shear and bending performance of carbon fiber composite sandwich panels with pyramidal truss cores. Acta Materialia 60, 1455–1466.
Xiong, J., Ma, L., Vaziri, A., Yang, J., Wu, L., 2012b. Mechanical behavior of carbon fiber composite lattice core sandwich panels fabricated by laser cutting. Acta Materialia 60, 5322–5334.
Xiong, J., Ma, L., Wu, L., Li, M., Vaziri, A., 2011a. Mechanical behavior of sandwich panels with hollow Al–Si tubes core construction. Materials and Design 32, 592–597.
Xiong, J., Ma, L., Wu, L., Liu, J., Vaziri, A., 2011b. Mechanical behavior and failure of composite pyramidal truss core sandwich columns. Composites Part B: Engineering 42, 938–945.
Xiong, J., Ma, L., Wu, L., Wang, B., Vaziri, A., 2010. Fabrication and crushing behavior of low density carbon fiber composite pyramidal truss structures. Composite Structures 92, 2695–2702.
Xue, Z., Hutchinson, J.W., 2004a. A comparative study of impulse-resistant metal sandwich plates. International Journal of Impact Engineering 30, 1283–1305.
Xue, Z., Hutchinson, J.W., 2004b. Constitutive model for quasi-static deformation of metallic sandwich cores. International Journal for Numerical Methods in Engineering 61, 2205–2238.
Xue, Z., Vaziri, A., Hutchinson, J.W., 2008. Material aspects of dynamic neck retardation. Journal of the Mechanics and Physics of Solids 56, 93–113.
Yang, P., Bifeng, S., 2006. Solving the combinatorial explosion problem when calculating the multiple-hit vulnerability of aircraft. Journal of aircraft 43, 5.
Yang, P., Bifeng, S., Qing, H., Baiyu, O., 2009. A direct simulation method for calculating multiple-hit vulnerability of aircraft with overlapping components. Chinese Journal of Aeronautics 22, 612–619.